mining

MDPI

Article

On the Behavior of Bauxite Tailings under a Wide Range of Stresses

Rosanne Rodrigues Santos Maciel Gonçalves, Matheus de Rezende Dutra, Bruna Zakharia Hoch, Hugo Carlos Scheuermann Filho, Fernando Schnaid and Lucas Festugato *

Graduate Program in Civil Engineering, Universidade Federal do Rio Grande do Sul, Porto Alegre 90035-190, RS, Brazil; santosrosanne@hotmail.com (R.R.S.M.G.); rdutra.matheus@gmail.com (M.d.R.D.); brunahoch@gmail.com (B.Z.H.); hugocsf@ufrgs.br (H.C.S.F.); fernando@ufrgs.br (F.S.)

* Correspondence: lucas@ufrgs.br

Abstract: Despite its vital importance to the contemporary economy, some drawbacks are mainly associated with waste derived from mining activity. This waste consists of tailings that are hydraulically disposed of in large impoundments, the tailings dams. As the dams are enlarged to accommodate higher amounts of materials, the stress states at which the deposited tailings are submitted change. This may be a concern for the stability of such structures once the geotechnical behavior of this material may be complex and challenging to predict, considering the existing approaches. Thus, the present study concerns the mechanical response of bauxite tailings under a wide span of stresses, ranging from 25 kPa to 4000 kPa. One-dimensional compression tests and isotropically drained and undrained triaxial tests were carried out on intact and remolded samples of the bauxite tailings. The after-shearing grain size distribution was characterized via sedimentation analysis. The results have shown a stress-dependency of the critical state friction angle for the intact material, which may be related to fabric alterations derived from structure deterioration and particle breakage. Overall, this research provides valuable insights into the response of structured and de-structured bauxite tailings, which are helpful for future constitutive modeling of such material.

Keywords: laboratory tests; silts; stress analysis; stress path; tailings; bauxite tailings

Citation: Gonçalves, R.R.S.M.; de Rezende Dutra, M.; Hoch, B.Z.; Scheuermann Filho, H.C.; Schnaid, F.; Festugato, L. On the Behavior of Bauxite Tailings under a Wide Range of Stresses. *Mining* **2024**, *4*, 629–641. https://doi.org/10.3390/mining4030035

Received: 21 June 2024
Revised: 14 August 2024
Accepted: 29 August 2024
Published: 31 August 2024

1. Introduction

Mining, a cornerstone of the modern economy, has experienced exponential growth since the first Industrial Revolution. It plays a crucial role in providing the inputs and supplies necessary for industrial activities, thereby driving economic development. This global expansion of mining activities underscores its significant impact on various sectors and regions, which are often unfavorable since the increased demand for metal ores, associated with the need to explore low-grade ores, has augmented waste generation derived from ore extraction and processing [1,2].

The waste of metal ores (e.g., iron ore, bauxite ore, and copper) beneficiation is termed tailings; it is usually a slurry containing crushed rock fines, chemicals, and elevated amounts of water. In other words, tailings are clastic and anthropic materials whose grading and mineralogy highly depend on the parental rock and the utilized beneficiation processes conferring unique characteristics (i.e., particle shape and surface texture) compared to natural soils of similar grading [3,4]. Over the past decades, tailings were usually hydraulically disposed of in vast impoundments, the tailings dams, where they progressively sediment and consolidate under their weight. Those were routinely expanded to store higher amounts of tailings: in Brazil, for example, there are 48 dams with a height greater than 60 m [5]. Most of them were expanded using the upstream method.

The recent legislation in Brazil, which forbids the construction of new upstream heightened dams and demands the de-characterization of existing ones, underscores the practical

relevance of this research. Understanding the mechanics of tailings is crucial for their safe and stable management. This understanding is based on considering the material's response under realistic stress levels, which commonly vary from 800 kPa to 10,000 kPa (Coop et al. 1992) [6]. The non-linearity related to particle breakage at higher stresses, which may appear on the critical state line (CSL), further emphasizes the practical implications of this study [7,8].

Several researchers have studied the utilization of bauxite tailings as alternative construction materials [9–12]. Also, some studies have evaluated the behavior of stabilized bauxite tailings with cement-like materials for dry stacking purposes. Ref. [13] assessed the parameters controlling the stiffness and loss of mass degradation of compacted bauxite tailings-alkali activated binder using a durability test procedure. Ref. [14] evaluated the leaching response of bauxite tailings stabilized with an alkali-activated cement. Both studies utilized green cement based on sugarcane bagasse ash, carbide lime, and sodium hydroxide. Nevertheless, there is a lack of studies concerning the mechanical response of bauxite tailings in conditions commonly encountered in tailings dams.

The present work evaluates the mechanical response of bauxite tailings under effective confining pressures ranging from 25 kPa to 4,000 kPa; it analyses the results in light of the Critical State Soil Mechanics [15,16]. This path is associated with a stress range capable of emulating conditions in real bauxite tailings dams. Possible fabric-related effects were assessed by comparing the response of undisturbed samples to the behavior of remolded specimens. The possibility of grain breakage was also investigated for some specimens. Overall, this study provides a valuable (and novel) framework for modeling the behavior of structured and de-structured bauxite tailings, which is of prime importance for safely designing and maintaining bauxite tailings dams.

2. Materials and Methods

The bauxite tailings (red mud) were collected from a dam situated in Brazil using Shelby tubes, which enable the collection of undisturbed samples. A total of ten tubes were used, and the samplings occurred at different locations of the dam but at the same depth. For each tube, the specific gravity (G_s) was individually measured by ASTM D854 [17]. The grain size distribution was evaluated for tubes 1, 2, 6, 4, 8, and 10 via sedimentation analysis following ASTM D7928 [18]. The Atterberg limits were assessed in agreement with ASTM D4318 [19]. Those results are summarized in Table 1, whereas Figure 1 depicts the grain size distribution curves, which attest to a similar gradation between the samples retrieved from different tubes. According to the Unified Soil Classification System, the bauxite tailings are classified as lean clay (CL) [20]. The undisturbed sample's void (e) ratio was approximately 1.20; the moisture content (w) was around 30%. Mineralogically, X-ray diffraction (XRD, Rigaku®, Porto Alegre-RS, Brazil) tests have attested to the presence of Hematite, Gibbsite, and Goethite. Chemically. Chemically, the material is mainly composed of aluminum (Al), silicon (Si), iron (Fe), sodium (Na), and titanium (Ti), as demonstrated by the X-ray fluorescence (XRF, PanAlytical MDP Shimadzu XRF1800®, Porto Alegre-RS, Brazil) test. XRD and XRF tests followed the procedures stated in [21,22].

Table 1. Physical characteristics of the bauxite tailings.

Physical Properties	Mean Value	Test Method
Specific gravity [1]	3.01	ASTM D854
Plastic limit—PL (%)	23	ASTM D4318
Liquid limit—LL (%)	32	
Plastic index—PI (%)	9	
Coarse Sand [1] (2.00 mm < diameter < 4.75 mm) (%)	0	ASTM D7928
Medium Sand [1] (0.425 mm < diameter < 2.00 mm) (%)	0	
Fine Sand [1] (0.075 mm < diameter < 0.425 mm) (%)	9	
Silt [1] (0.002 < diameter < 0.075 mm) (%)	73	
Clay [1] (diameter < 0.002 mm) (%)	18	

[1]—mean values

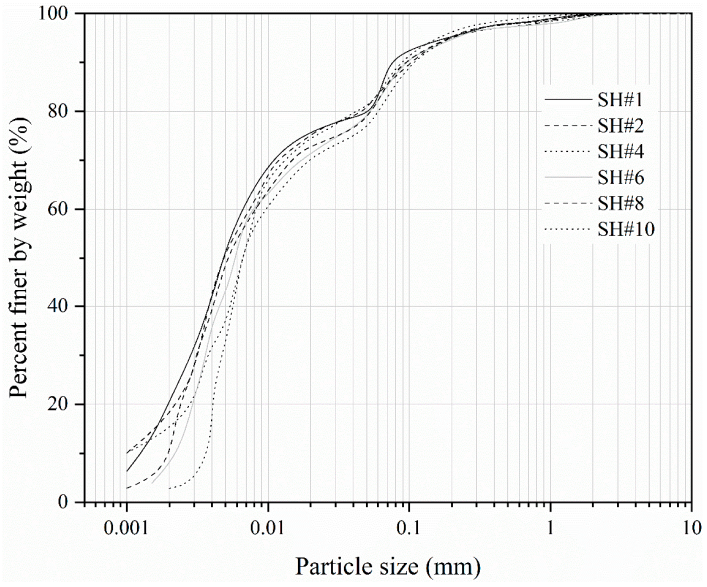

Figure 1. Bauxite tailings grain size distribution.

3. One-Dimensional Compression Tests

The 1D compression test allows the material's stress-strain response owing to one-dimensional compression, enabling valuable insights concerning the bauxite tailings using a relatively simple procedure. These tests were carried out by ASTM D2435 standard [23] using intact and remolded specimens (50 mm in diameter and 20 mm in height). The remolded samples were directly compacted into the test ring to the same void ratio of the intact material (e = 1.20) and using the same moisture content (w = 30%). Filter paper slices were placed on both sides of the test ring before allocating the sample between two porous stones in the oedometer cell, which was then filled with distilled water. Loading stages of 50, 100, 200, 400, 1000, 2000, and 4000 kPa were applied, followed by two unloading phases of 4000 kPa and 2000 kPa. Each load increment (or decrement) was maintained for a minimum interval of 24 h. During the test, the vertical displacement was electronically monitored using a Linear Variable Differential Transformer (LVDT, Novotechnik®, Porto Alegre-RS, Brazil) positioned in contact with the top cap of the test ring.

4. Triaxial Tests

The triaxial compression tests enable understanding of the geomaterial's response (e.g., stress-strain, and volume change response) under different stress conditions that can emulate the bauxite tailings' on-field stress states. Table 2 summarizes the characteristics of the isotropically consolidated drained (CID) and isotropically consolidated undrained (CIU) triaxial tests conducted per ASTM D7181 [24] and ASTM D4767 [25]. Both used fully saturated cylindrical samples (50 mm in diameter and 100 mm in height). The intact specimens were carefully trimmed to attain the prescribed dimensions; the reconstituted samples were fabricated using the moist-tamping technique [26] inside a cylindrical split mold where six moist layers were manually tamped to the assigned void ratio. A latex membrane (utilized for the triaxial tests) circumscribed the mold. The test specimens were submitted to CO_2 and distilled water percolation, followed by the constant rate backpressure increment (maintaining the mean effective stress equal to 20 kPa) up to obtaining a B-value greater than 0.98. The consolidation stage consisted of augmenting the chamber pressure to the desired effective confining pressure at 1 kPa per minute. The shearing was strain-controlled and conducted at 4 mm per hour. The cell pressure and the backpressure were digitally monitored using pressure transducers and controlled using advanced pressure volume controllers; a load cell electronically monitored the axial load. Locally, Hall effect sensors, positioned directly in contact with the test specimen (axial and radial measurements), enabled displacement measurements throughout all the phases of

the tests [27]. Globally, a linear variable differential transformer (fixated externally to the chamber) measured the axial displacement during the shearing phase. Also, a volume gauge permitted the assessment of the volumetric variation through the flow volume of water on/from the sample.

Table 2. Summary of test characteristics.

	Tests	Shear Condition	Sample	Shelby	p'_0
1	Triaxial Test	CIU	R	SH #1	25 kPa
2			U		
3			U		50 kPa
4			R	SH #8	100 kPa
5			U		
6			U		400 kPa
7			R	SH #5	
8			R	SH #8	1000 kPa
9			U	SH #4	
10			R	SH #6	2000 kPa
11			U		
12			R	SH #2	4000 kPa
13			U		
14		CID	U	SH #4	1000 kPa
15			U	SH #6	2000 kPa
16			U	SH #2	4000 kPa
1	One-Dimensional Compression		U	SH #1	4000 kPa
2			R	SH #8	4000 kPa

CIU—Undrained Tests; CID—Drained Tests; U—Undisturbed Specimens R—Remolded Specimens.

5. Results

Figure 2 displays the one-dimensional compression response for intact and remolded bauxite tailings specimens. Fabric differences arising from the specimen's remolding have incurred two non-convergent normal compression lines (NCLs), considering the vertical stress (σ'_v) range utilized herein. The final differences in the specific volume (ν) values reinforce this trend. Perhaps the NCLs would converge towards a single line for greater stress levels capable of erasing any initial fabric differences decurrent from the remolding process [28,29]. Moreover, the intact samples were slightly stiffer than the remolded ones at lower stresses. Such a trend may indicate the existence of a structure in the intact (undisturbed) material that erases at low-pressure levels [30,31].

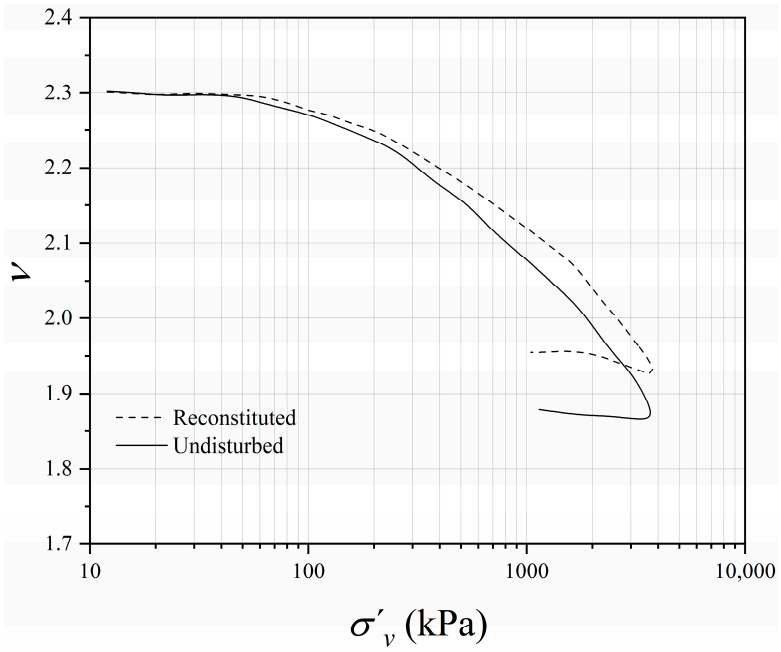

Figure 2. One-dimensional behavior.

6. Shearing Behavior in the Triaxial Tests

Figure 3a shows the intact specimens of the bauxite tailing used in the triaxial tests; Figure 3b depicts the reconstituted sample. Figure 4a displays the stress-strain response and pore pressure variation for the CIU tests conducted under low initial effective confining pressures (p'_0 = 25 kPa, 100 kPa, and 400 kPa) on intact and remolded samples; Figure 4b displays the same data for the higher pressures (p'_0 = 1000 kPa, 2000 kPa, 4000 kPa). Figure 4c exhibits the triaxial testing data for CID tests carried out using undisturbed samples (p'_0 = 1000 kPa, 2000 kPa, and 4000 kPa). Most of the tested specimens have shown a ductile behavior accompanied by a contractive trend (or positive pore pressure variation). At lower stress levels ($p'_0 \leq$ 400 kPa), the intact specimens were strengthener and initially stiffer than the remolded ones, indicating that the original (undisturbed) fabric contributed to such a response. In other words, a slightly bonded structure appears to exist in the undisturbed material and has remained undamaged during the consolidation at pressures below 100 kPa [32,33]. This explains the slightly dilatative trend (i.e., negative pore pressure variation) reported for the undisturbed specimen sheared at 25 kPa. For greater confining pressures, the remolded and undisturbed samples presented a contractive tendency during shearing, but the latter were initially stiffer at lower stresses.

(**a**)

(**b**)

Figure 3. Samples used in the triaxial tests: (**a**) intact; (**b**) remolded.

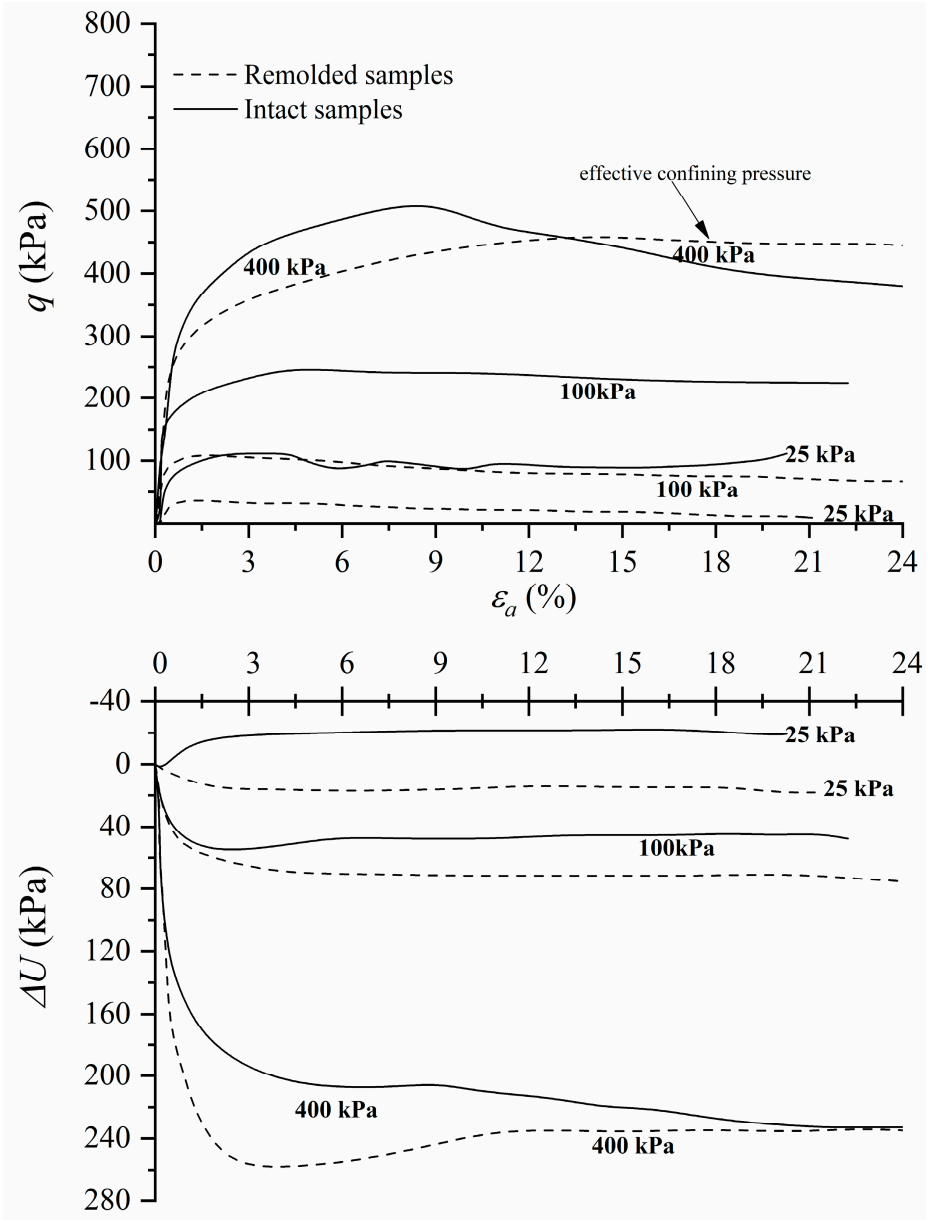

Figure 4. *Cont.*

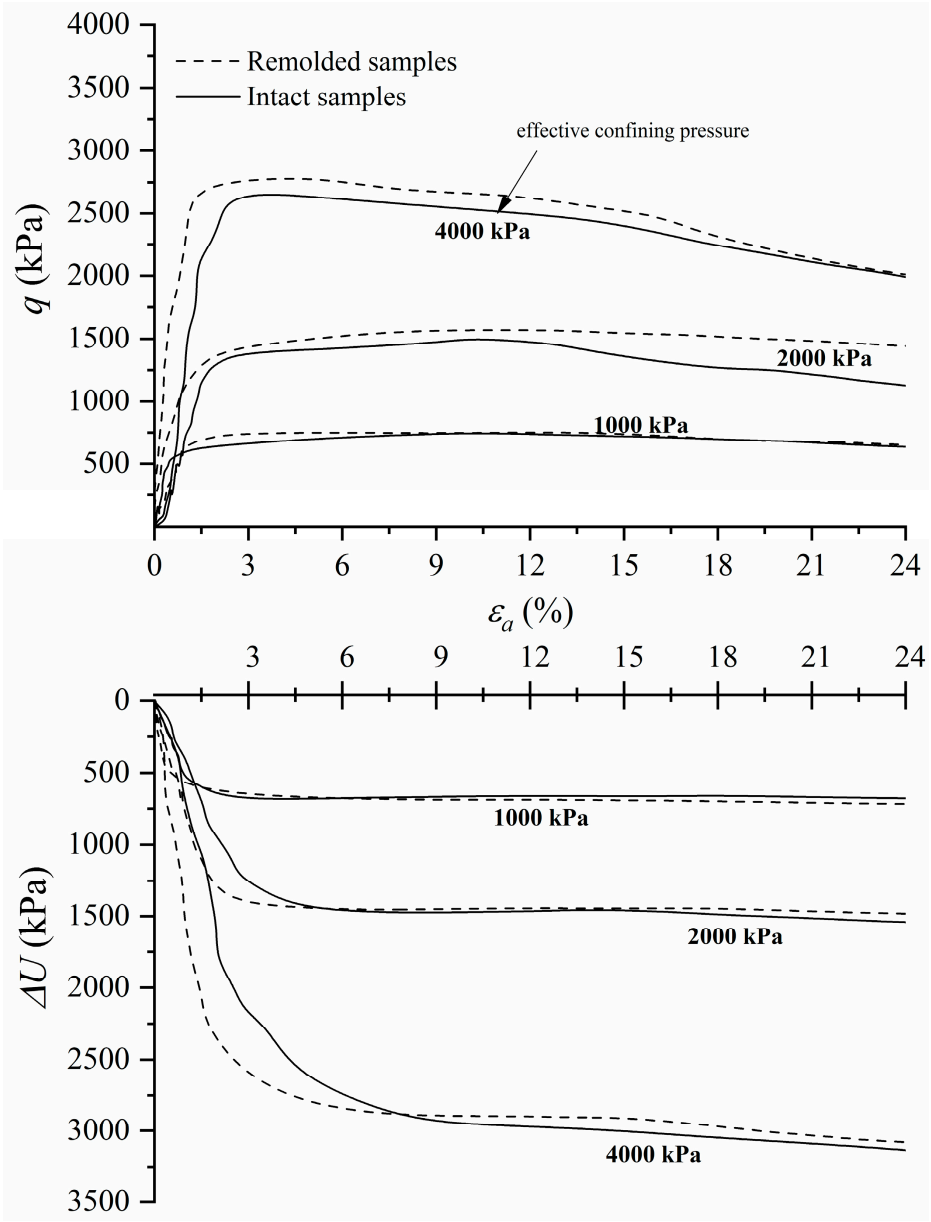

Figure 4. *Cont*.

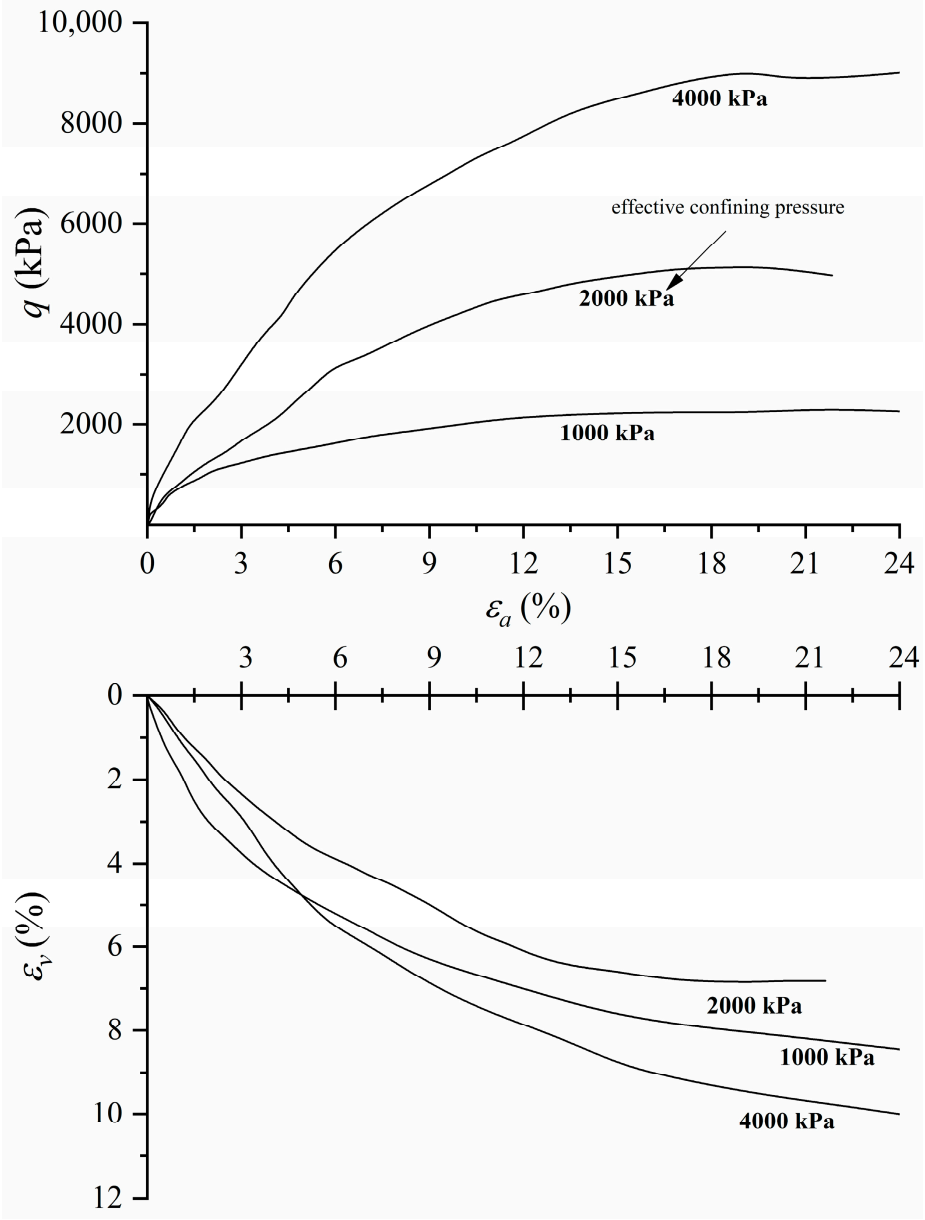

Figure 4. Triaxial test of bauxite tailings: (**a**) CIU for lower stress range; (**b**) CIU for higher stress range; (**c**) CID tests.

7. Stress Paths and Critical States

Figure 5 depicts the stress paths over the entire stress range, emphasizing the lower stress region. Even though the critical state, characterized by the steadiness on both the deviatoric stress and the pore pressure variation (or volumetric strain), may not have been reached on some of the tests, the authors used the endpoints to fit a critical state envelope. All of the triaxial testing data yielded a critical state line in the effective stress plane q:p' having a slope of M_{TC} = 1.32 (φ'_{cs} = 32.6°); the tests conducted at lower stresses resulted in M_{tc} = 1.43 (φ'_{cs} = 35.3°). This phase change is likely associated with fabric from the weak bonds in the intact material, which erases in the consolidation phase at higher pressures. Once the shear proceeds, the particles rearrange; particle breakage may occur at higher stresses [34–36]. Therefore, a lower critical state friction angle should be used for higher depths in a tailings dam.

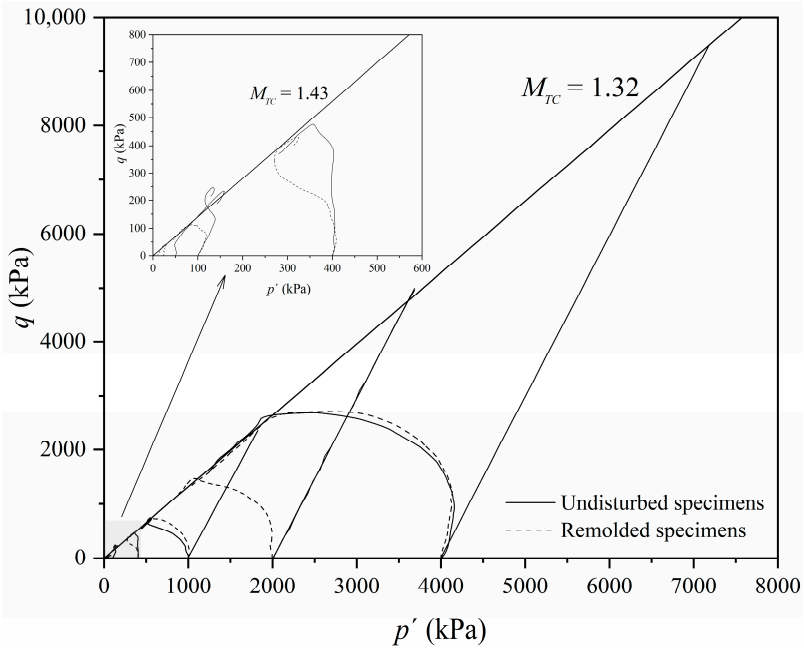

Figure 5. Stress paths in the effective stress plane.

Figure 6 presents the stress paths in the compression plane v:$ln\ p'$, where a curved shape critical state line [37] fits the test endpoints using the following equation:

$$v = a - b\left(\frac{p'}{100\ \text{kPa}}\right)^{c} \quad (1)$$

where a, b, and c are fitting parameters that depend on the material's characteristics (a = 2.37, b = 0.20, and c = 0.36). All the tests but three converged towards the critical state line during the shearing; the non-convergence occurred on undisturbed samples sheared under lower confining levels. The bonded structure has possibly altered the dynamics of the volume change trend (i.e., dilatant instead of compressive), a typical response of artificially cemented soils compared to uncemented soils tested under the same conditions [38–40].

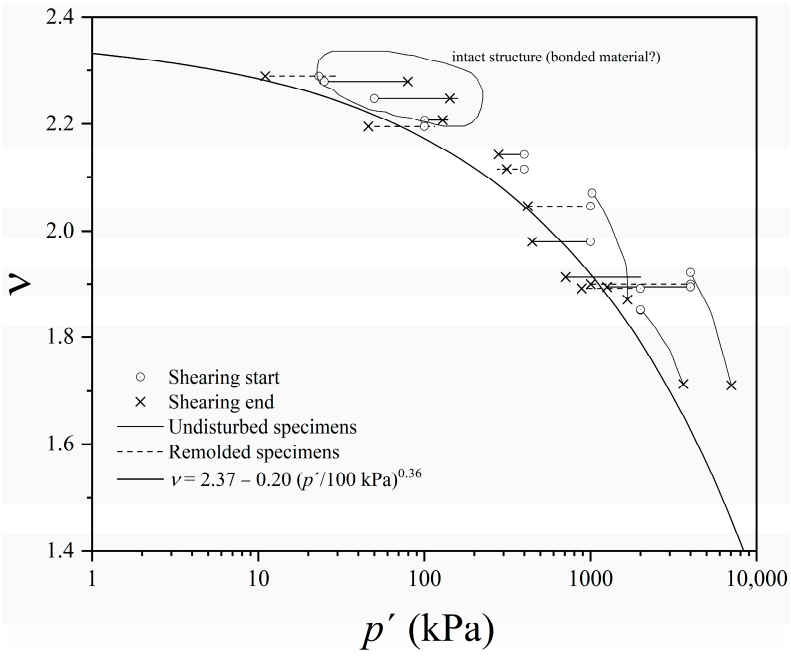

Figure 6. Stress paths in the volumetric plane.

8. Grain Size Analysis

Figure 7 presents the after-shearing grain size distribution for triaxial tests conducted at initial effective confining pressures of 2000 kPa (Figure 7a) and 4000 kPa (Figure 7b). Also, the grain size distribution of the untested material is plotted in each graph. The bauxite tailings became finer owing to the combined effect of the consolidation and the shearing phases of the triaxial tests. An augment in the clay fraction, accompanied by a decrement in the silt fraction, is observable by comparing the grain size distribution curves of the tested and untested tailings. Quantitatively, the particle breakage factor—B_f can provide insight into the extension of particle breakage [41]. It is simply the difference between the finer particles' quantity after testing and the content of finer particles existing in the untested (natural) material. Table 3 summarizes the B_f values for the curves presented in Figure 7. In this regard, no trend relating to the drainage setup during the shear and/or the specimen's type can be established based on particle breakage.

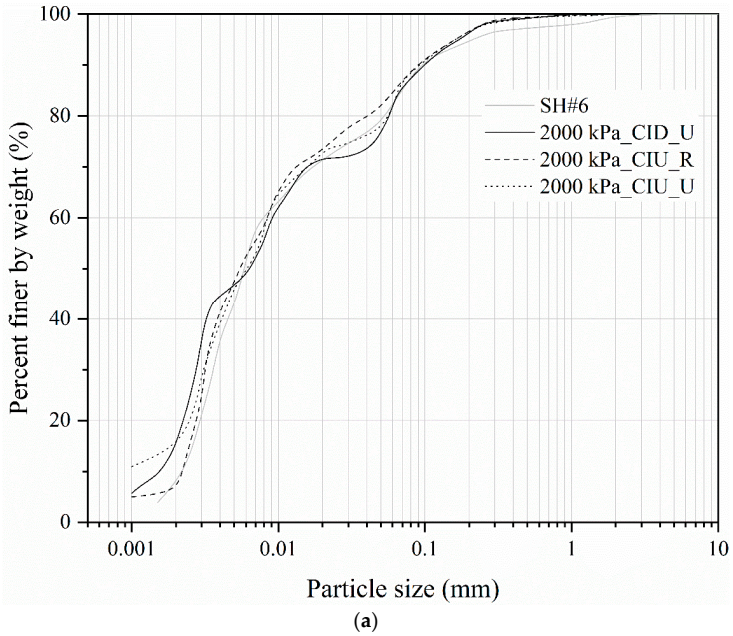

(**a**)

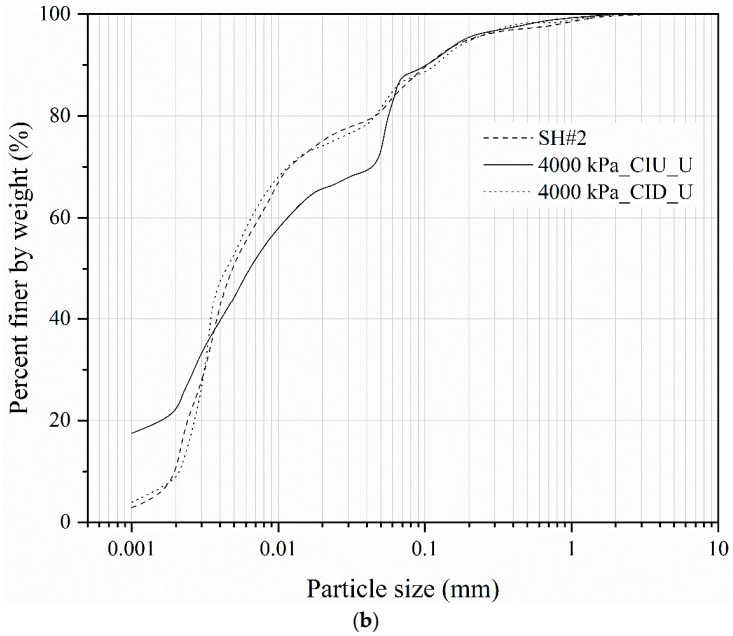

(**b**)

Figure 7. Grain size distribution after triaxial tests: (**a**) 2000 kPa, (**b**) 4000 kPa.

Table 3. Breakage factor.

P'_0 (kPa)	Shearing	Sample	B_f
2000	U	REM	0.02
2000	U	UND	0.07
2000	D	UND	0.05
4000	U	UND	0.03
4000	D	UND	0.15

B_f—particle breakage factor.

9. Conclusions

This paper evaluated the mechanical response of bauxite tailings over a wide range of confining pressures through triaxial compression tests conducted on undisturbed and remolded specimens. Overall, the results showed differences in the behavior of the intact and remolded specimens at lower stress levels ($p_0' < 400$ kPa), which may be related to the existence of a weak bonded structure in the intact material that strengthens and stiffens it. The studied bauxite tailings became finer through the combined effect of consolidation and shearing over triaxial testing. An increase in the clay fraction, accompanied by a decrement in the silt fraction, was observable by comparing the grain size distribution curves of the tested and untested tailings.

Also, a bi-linear trend was found considering the critical state envelopes in the effective stress plane, incurring a stress-dependent critical state friction angle value ($\varphi'_{cs} = 35.3^\circ$ for $p' < 400$ kPa and $\varphi'_{cs} = 32.6^\circ$ for the entire stress range). In the volumetric plane ν: ln p', a curved-shape critical state line fitted the test endpoints: all but three tests converged towards the fitted curve; those three were undisturbed samples sheared under low-stress levels, indicating that the bonded structure may have altered the dynamics of the volume change trend (dilatant rather than compressive).

In addition, future research is necessary to enlarge the comprehension of the behavior of bauxite tailings under other boundary conditions involving confining pressures and imposed stress paths. Alternative stress paths rather than conventional triaxial compression would enlighten the understanding of the tailings response, particularly considering the location of the failure and critical state envelopes, as well as the role of the intermediate principal stress on the tailings response. A detailed microstructure evaluation is also necessary to explain the fabric features of the intact and remolded specimens.

Author Contributions: Conceptualization, R.R.S.M.G., L.F. and F.S.; methodology, R.R.S.M.G.; testing and data analysis, R.R.S.M.G., B.Z.H. and M.d.R.D.; writing—original draft preparation, H.C.S.F. and L.F.; writing—review and editing, H.C.S.F. and L.F. All authors have read and agreed to the published version of the manuscript.

Funding: This research was funded by the Brazilian Research Council CNPq (grants # 402572/2021-1 and 307286/2022-3).

Data Availability Statement: Some or all data, models, or codes that support the findings of this study are available from the corresponding author upon reasonable request.

Acknowledgments: The authors thank the Brazilian Research Council CNPq for supporting the research group.

Conflicts of Interest: The authors declare no conflict of interest.

List of Notations

B_f	breakage factor
e	void ratio; void ratio for undisturbed sample
e_{max}	maximum void ratio
e_{min}	minimum void ratio
p'	mean effective stress

q	deviatoric stress
CSL	critical state line
LL	liquid limit
NCL	normal compression line
ICL	isotropic compression line
PI	plasticity index
PL	plasticity limit
ε_a	axial strain
SG	specific gravity of solids
ν	specific volume
σ'_v	effective vertical stress
ϕ'_{cs}	critical state angle of friction
R	remolded
U	undisturbed

References

1. IBRAM—Instituto Brasileiro de Mineração. *Gestão E Manejo de Rejeitos de Mineração*; IBRAM: Brasilia, Brazil, 2016; ISBN 978-85-61993-10-8.
2. Nkuna, R.; Ijoma, G.N.; Matambo, T.S.; Chimwani, N. Accessing Metals from Low-Grade Ores and the Environmental Impact Considerations: A Review of the Perspectives of Conventional versus Bioleaching Strategies. *Minerals* **2022**, *12*, 506. [CrossRef]
3. Kossoff, D.; Dubbin, W.E.; Alfredsson, M.; Edwards, S.J.; Macklin, M.G.; Hudson-Edwards, K.A. Mine Tailings Dams: Characteristics, Failure, Environmental Impacts, and Remediation. *Appl. Geochem.* **2014**, *51*, 229–245. [CrossRef]
4. Silva, J.P.S.; Rissoli, A.L.C.; Cacciari, P.P.; da Fonseca, A.J.P.V.; Filho, H.C.S.; Wagner, A.C.; Carvalho, J.V.d.A.; Festugato, L.; Consoli, N.C. Triaxial Testing Response of Compacted Iron Ore Tailings Considering a Broad Spectrum of Confining Pressures. *Soils Found.* **2024**, *64*, 101438. [CrossRef]
5. ANM—Agência Nacional de Mineiração Cadastro Nacional. *Sistema de Gestão de Segurança de Barragens de Mineração—SIGBM*; ANM: Brasília, Brazil, 2021.
6. Coop, M.R.; Lee, I.K.; Houlsby, G.T.; Schofield, A.N. The Behaviour of Granular Soils at Elevated Stresses. In Proceedings of the Wroth Memorial Symposium Held at St Catherine's College, Oxford, UK, 27–29 July 1992; Thomas Telford: Oxford, UK, 1992.
7. Bedin, J.; Schnaid, F.; Da Fonseca, A.V.; Costa Filho, L.D.M. Gold Tailings Liquefaction under Critical State Soil Mechanics. *Géotechnique* **2012**, *62*, 263–267. [CrossRef]
8. Li, W.; Coop, M.R.; Senetakis, K.; Schnaid, F. The Mechanics of a Silt-Sized Gold Tailing. *Eng. Geol.* **2018**, *241*, 97–108. [CrossRef]
9. De Azevedo, A.R.G.; Marvila, M.T.; De Oliveira, M.A.B.; Umbuzeiro, C.E.M.; Huaman, N.R.C.; Monteiro, S.N. Perspectives for the Application of Bauxite Wastes in the Development of Alternative Building Materials. *J. Mater. Res. Technol.* **2022**, *20*, 3114–3125. [CrossRef]
10. Nascimento, R.S.; Corrêa, J.A.M.; Figueira, B.A.M.; Pinheiro, P.A.; Silva, J.H.; Freire, P.T.C.; Quaranta, S. From Mining Waste to Environmetal Remediation: A Nanoadsorbent from Amazon Bauxite Tailings for the Removal of Erythrosine B Dye. *Appl. Clay Sci.* **2022**, *222*, 106482. [CrossRef]
11. Ou, X.; Chen, S.; Jiang, J.; Qin, J.; Zhang, L. Reuse of Red Mud and Bauxite Tailings Mud as Subgrade Materials from the Perspective of Mechanical Properties. *Materials* **2022**, *15*, 1123. [CrossRef]
12. Singh, V.; Bano, S.; Chauhan, V.B.; Pal, P.; Kumar, A.; Srivastava, J.B. Red Mud as a Sustainable Road Construction Material: An Experimental Investigation. *Constr. Build. Mater.* **2024**, *411*, 134549. [CrossRef]
13. Bruschi, G.J.; dos Santos, C.P.; Tonini de Araújo, M.; Ferrazzo, S.T.; Marques, S.F.V.; Consoli, N.C. Green Stabilization of Bauxite Tailings: Mechanical Study on Alkali-Activated Materials. *J. Mater. Civ. Eng.* **2021**, *33*, 06021007. [CrossRef]
14. Bruschi, G.J.; Dos Santos, C.P.; Levandoski, W.M.K.; Ferrazzo, S.T.; Korf, E.P.; Saldanha, R.B.; Consoli, N.C. Leaching Assessment of Cemented Bauxite Tailings through Wetting and Drying Cycles of Durability Test. *Environ. Sci. Pollut. Res.* **2022**, *29*, 59247–59262. [CrossRef] [PubMed]
15. Atkinson, J. *An Introduction to the Mechanics of Soils and Foundations: Through Critical State Soil Mechanics*; McGraw-Hill International Series in Civil Engineering; McGraw-Hill Book Co.: London, UK; New York, NY, USA, 1993; ISBN 978-0-07-707713-6.
16. Atkinson, J.H.; Bransby, P.L. *The Mechanics of Soils: An Introduction to Critical State Soil Mechanics*; Indo American Books: Delhi, India, 2012; ISBN 978-93-82661-06-1.
17. *ASTM D854*; ASTM Test Methods for Specific Gravity of Soil Solids by Water Pycnometer. ASTM International: West Conshohocken, PA, USA, 2014.
18. *ASTM D7928*; ASTM Test Method for Particle-Size Distribution (Gradation) of Fine-Grained Soils Using the Sedimentation (Hydrometer) Analysis. ASTM International: West Conshohocken, PA, USA, 2021.
19. *ASTM D4318*; ASTM Test Methods for Liquid Limit, Plastic Limit, and Plasticity Index of Soils. ASTM International: West Conshohocken, PA, USA, 2017.
20. *ASTM D2487*; ASTM Practice for Classification of Soils for Engineering Purposes (Unified Soil Classification System). ASTM International: West Conshohocken, PA, USA, 2017.

21. De Villiers, J.P.R.; Lu, L. XRD Analysis and Evaluation of Iron Ores and Sinters. In *Iron Ore*; Elsevier: Amsterdam, The Netherlands, 2015; pp. 85–100, ISBN 978-1-78242-156-6.
22. Buhrke, V.E.; Jenkins, R.; Smith, D.K. (Eds.) *A Practical Guide for the Preparation of Specimens for X-ray Fluorescence and X-ray Diffraction Analysis*; Wiley-VCH: New York, NY, USA, 1999; ISBN 978-0-471-19458-3.
23. *ASTM D2435*; ASTM Test Methods for One-Dimensional Consolidation Properties of Soils Using Incremental Loading. ASTM International: West Conshohocken, PA, USA, 2011.
24. *ASTM D7181*; ASTM Test Method for Consolidated Drained Triaxial Compression Test for Soils. ASTM International: West Conshohocken, PA, USA, 2020.
25. *ASTM D4767*; ASTM Test Method for Consolidated Undrained Triaxial Compression Test for Cohesive Soils. ASTM International: West Conshohocken, PA, USA, 2020.
26. David Suits, L.; Sheahan, T.; Frost, J.; Park, J.-Y. A Critical Assessment of the Moist Tamping Technique. *Geotech. Test. J.* **2003**, *26*, 9850. [CrossRef]
27. Clayton, C.R.I.; Khatrush, S.A. A New Device for Measuring Local Axial Strains on Triaxial Specimens. *Géotechnique* **1986**, *36*, 593–597. [CrossRef]
28. Hong, Z.-S.; Yin, J.; Cui, Y.-J. Compression Behaviour of Reconstituted Soils at High Initial Water Contents. *Géotechnique* **2010**, *60*, 691–700. [CrossRef]
29. Carrion, M.A.; Coop, M.R.; Nocilla, A. Assessment of the Effects of the Structure on the Compression Behaviour of a Young Alluvial Silty Soil. *Soils Found.* **2019**, *59*, 1024–1036. [CrossRef]
30. Rotta, G.V.; Consoli, N.C.; Prietto, P.D.M.; Coop, M.R.; Graham, J. Isotropic Yielding in an Artificially Cemented Soil Cured under Stress. *Géotechnique* **2003**, *53*, 493–501. [CrossRef]
31. Zhang, F.; Jiang, M. Do the Normal Compression Lines of Cemented and Uncemented Geomaterials Run Parallel or Converge to Each Other after Yielding? *Eur. J. Environ. Civ. Eng.* **2021**, *25*, 368–386. [CrossRef]
32. Leroueil, S.; Vaughan, P.R. The General and Congruent Effects of Structure in Natural Soils and Weak Rocks. *Géotechnique* **1990**, *40*, 467–488. [CrossRef]
33. Cuccovillo, T.; Coop, M.R. Yielding and Pre-Failure Deformation of Structured Sands. *Géotechnique* **1997**, *47*, 491–508. [CrossRef]
34. Bandini, V.; Coop, M.R. The Influence of Particle Breakage on the Location of the Critical State Line of Sands. *Soils Found.* **2011**, *51*, 591–600. [CrossRef]
35. Ghafghazi, M.; Shuttle, D.A.; DeJong, J.T. Particle Breakage and the Critical State of Sand. *Soils Found.* **2014**, *54*, 451–461. [CrossRef]
36. Tong, C.-X.; Zhai, M.-Y.; Li, H.-C.; Zhang, S.; Sheng, D. Particle Breakage of Granular Soils: Changing Critical State Line and Constitutive Modelling. *Acta Geotech.* **2022**, *17*, 755–768. [CrossRef]
37. Jefferies, M.; Been, K. *Soil Liquefaction: A Critical State Approach*, 2nd ed.; CRC Press: Boca Raton, FL, USA, 2015; ISBN 978-0-429-15391-4.
38. Schnaid, F.; Prietto, P.D.M.; Consoli, N.C. Characterization of Cemented Sand in Triaxial Compression. *J. Geotech. Geoenviron. Eng.* **2001**, *127*, 857–868. [CrossRef]
39. Lade, P.V.; Overton, D.D. Cementation Effects in Frictional Materials. *J. Geotech. Engrg.* **1989**, *115*, 1373–1387. [CrossRef]
40. Lade, P.V.; Trads, N. The Role of Cementation in the Behaviour of Cemented Soils. *Geotech. Res.* **2014**, *1*, 111–132. [CrossRef]
41. Nakata, A.F.L.; Hyde, M.; Hyodo, H.; Murata. A Probabilistic Approach to Sand Particle Crushing in the Triaxial Test. *Géotechnique* **1999**, *49*, 567–583. [CrossRef]